The effect of initial molecular weight on the structural evolution of Polyamide 1012 during high-temperature thermal treatments as revealed by Successive Self-Nucleation and Annealing

Xuan Li,[1,2] Xueting Li,[3] Yu Wang[1], Ping Zhu[1], Dujin Wang,[1,2] Alejandro J. Müller,[4,5,] and Xia Dong[1,2,]**

[1]Beijing National Laboratory for Molecular Science, CAS Key Laboratory of Engineering Plastics, Institute of Chemistry, Chinese Academy of Sciences, Beijing 100190, P. R. China

[2]University of Chinese Academy of Sciences, Beijing 100049, P. R. China

[3]Shandong Guangyin New Material Co., Ltd., Zibo, Shandong Province 255022, P. R. China

[4]POLYMAT and Department of Polymers and Advanced Materials: Physics, Chemistry and Technology, Faculty of Chemistry, University of the Basque Country UPV/EHU, Paseo Manuel de Lardizabal 3, Donostia-San Sebastián 20018, Spain

[5]Ikerbasque, Basque Foundation for Science, Plaza Euskadi 5, Bilbao 48009, Spain

*Corresponding authors: alejandrojesus.muller@ehu.es and xiadong@iccas.ac.cn

The effect of initial molecular weight on the structural evolution of Polyamide 1012 during high-temperature thermal treatments as revealed by Successive Self-Nucleation and Annealing

Xuan Li,[1,2] Xueting Li,[3] Yu Wang[1], Ping Zhu[1], Dujin Wang,[1,2] Alejandro J. Müller,[4,5,] and Xia Dong[1,2,]**

For Table of Contents use only

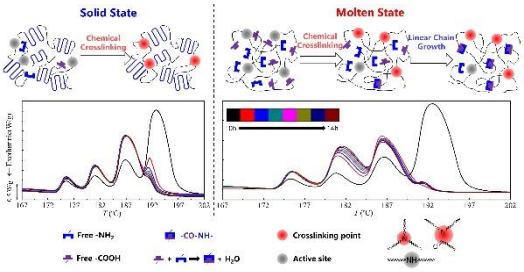

ABSTRACT: Successive self-nucleation and annealing (SSA) can thermally fractionate semi-crystalline polymers, thus detecting the characteristic structural features that lead to specific melting point distributions (corresponding to the lamellar thickness distribution in the sample). SSA has been employed to investigate the structural evolution of polyamide 1012 (PA1012) when it is submitted to thermal treatments in the solid-state (below the melting point, T_m) as well as in the liquid-state (above T_m), as a function of the molecular weight of the sample. Below T_m, mainly chemical crosslinking occurred, thus provoking the decrease in the melting enthalpy of the highest temperature SSA melting fraction. The structural evolution was limited primarily by crystallization, and the high crystallinity of the low molecular weight samples led to low crosslinking rates. Above T_m, the structural evolution was correlated with the melt viscosity and the end group concentration. The concentration and diffusion ability of end groups was inversely proportional to the initial melt viscosities, therefore linear chain growing rate increased with the decrease in initial melt viscosities. Crosslinking reaction rate increased with the increase in initial melt viscosities. This work has determined the structural evolution differences of PA1012 depending on different initial states. This work can provide guidance for studies of thermal structural evolution of all AABB-type polyamides and subsequent design of high-performance materials with various structures according to their application requirements.

KEYWORDS: PA1012; Chemical crosslinking; Linear chain growth; Successive self-nucleation and annealing (SSA).

INTRODUCTION

Polyamide 1012 (PA1012) is synthesized via condensation polymerization between dodecanedioic acid and decanediamine. Dodecanedioic acid can currently be obtained by biological fermentation methods, which are valuable for their environmentally friendly conversion processes with biobased materials under mild conditions. Decanediamine can be converted from decanedioic acid, which can also be obtained by biological fermentation methods. Therefore, PA1012 has been developing rapidly using monomer preparation technology based on biofermented sources.

A series of results have been reported on the crystalline structure of PA1012. Atkins et al.[1] analyzed the crystal structure and the crystal surface of PA1012 obtained by solution crystallization. They found that PA1012 crystals have adjacent re-entry chain folds that must be constituted by alkane chain segments. Yan et al.[2] prepared different PA1012 crystal forms by melt-crystallization, and by solution casting from meta-cresol and trifluoroacetic acid. It was found that melt-crystallized and samples cast from trifluoroacetic acid solution adopt α-form and γ-form, respectively. Different crystal forms (including α-form, γ-form and a mixture of these two) could grow from meta-cresol cast samples according to different cast temperatures. Yan et al.[3-5] observed a

double-melting phenomenon of PA1012 during DSC heating scans. They attributed the highest melting peak to the melting of recrystallized crystals during the heating scan, while the lowest melting endotherm was related to the melting of the lamellae formed during previous crystallization. Li et al. and Zhou et al. respectively studied the effects of hydrogen-bonding density and arrangement of amide groups on crystallization kinetics[6], dielectric behavior and the methylene infrared vibration[7].

As PA1012 material has been industrialized only recently, compared with PA11[8-11] and PA12[12-15], which have been commercialized for a long time, the research on PA1012 has been concentrated on structural evolution during stretching[16], shearing[17] or heating[18-19]. The external field and the chain structure can both affect the microstructure and the resultant physical properties in polyamides and its copolymers[20-21]. However, a key technical problem needs to be solved: What is the mechanism of structural change of PA1012 when submitted to thermal treatments at high temperatures for a specific period of time? For example, PA66 may be crosslinked[22] at high temperatures, as the effect of high temperature makes adjacent end-amino groups de-amine each other to produce secondary amino groups. The hydrogen atoms on the secondary amino group are more active and can react with the end amino or amide groups of other PA66 molecules to form a three-dimensional crosslinked network structure. Also, due to the characteristics of its polymerization process, the end groups of polyamides are still reactive in polymers which have already been polymerized and such activity can bring about structural changes upon heating in the subsequent processing, which is the reason

why it can undergo solid state polymerization (SSP)[23] via reactions of the chain end groups in the amorphous region, resulting in a secondary increase in molecular weight. For PA1012, these complex groups can have an impact on the structural changes during heat treatment at temperatures higher than the glass transition temperature (T_g), especially at those above $T_{m,onset}$, such as possible degradation and transamidation, resulting in unpredictable structural changes and possible properties deterioration. Here we chose 170 °C (close to $T_{m,onset}$) and 250 °C (highly above $T_{m,onset}$) to compare the structural evolution differences as a function of the molecular weight of PA1012, which were important in the actual processing.

This work is a continuation of our previous investigation[24] on the structural evolution of PA1012 subjected to high temperatures thermal treatments, using thermal fractionation as a tool to elucidate the structural changes that can occur during such treatments. Previous results[20] showed that when PA1012 is heated to high temperatures for a specific amount of time, it can undergo changes in physical and chemical structure depending on the temperature. We employed the successive self-nucleation and annealing (SSA) thermal fractionation method to follow the chemical structure evolution. Coupling SSA with heat treatments allowed tracing the *in situ* evolution of thermal fractions melting points (proportional to lamellar thicknesses)[25-28] of PA1012 during high-temperature thermal treatments. A competition between chain growth and crosslinking of PA1012 occurred during the high-temperature thermal treatments. Master curves of "time-temperature superposition" at a reference temperature were

constructed based on SSA results. The melting point distribution evolution (or lamellar thickness distribution evolution) was divided into three stages as a function of time. At shorter times (first stage) chemical crosslinking predominated. At intermediate times (second stage), the amount of end groups increased faster than before, and linear chain growth rapidly occurred along with the ongoing chemical crosslinking. Finally, at the last stage, linear chain growth predominated because of the increase in chain end-group reactions.

In this work, the differences in the structural evolution during high-temperature heat treatments in the solid state (below the melting point, T_m) and in the liquid state (above T_m) were investigated by employing PA1012 samples with different initial melt flow index (i.e., different initial molecular weights) depending on their different polymerization times. Below T_m, the structural evolution was mainly limited by crystallization. Above T_m, the structural evolution was associated with the diffusion and concentration of end groups. Based on our previous results[20], the present work has studied and characterized the structural evolution of PA1012s as a function of their initial molecular weight by SSA at different thermal treatment temperature ranges.

EXPERIMENTAL SECTION

Materials

The PA1012 pellets used in this research were provided by Shandong Guangyin New Material Co., Ltd. The melt flow index (MFI) of different PA1012 pellets were 1,

12, 18, 21, 43 g/10 min that were obtained according to the same formulation and process, depending on the difference in polymerization time. The fundamental physical characterization of the five kinds of PA1012 pellets is shown in Table 1. The different samples have been denoted according to their MFI value using the nomenclature S-MFI, for example S-12 is the PA1012 sample with MFI=12 g/10 min. The pellets were dried in a vacuum oven at 90 °C for 6 h before experiments.

Table 1. Fundamental physical characterization of PA1012 samples.

Sample	S-1	S-12	S-18	S-21	S-43
MFI [a] (g/10 min)	1	12	18	21	43
M_n [b] ($\times 10^4$ g/mol)	1.4	1.2	0.9	0.8	0.6
M_w [b] ($\times 10^4$ g/mol)	3.5	2.5	2.2	2.2	1.7
D [b]	2.53	2.16	2.52	2.55	2.86
T_m [c] (°C)	189.1	189.8	190.5	190.4	190.4
ΔH_m [c] (J/g)	19.5	24.0	27.1	31.4	40.5

[a] Determined by Melt Flow Indexer at 235 °C according to ASTM D1238 (2.16 kg). [b] Determined by GPC testing in HFiP mobile phase (40 °C). [c] Determined by DSC.

Gel Permeation Chromatography (GPC) Experiments

The mobile phase was hexafluoroisopropanol (HFiP), the test temperature was 40 ºC, and the concentration was 1 mg/mL. The molecular weight and their distribution is shown in Table 1 for all samples.

Differential Scanning Calorimetry (DSC)

TA Q2000 DSC instrument was employed for the following studies. The instrument was calibrated before measurements according to the experimental conditions to be used. All experimental samples were tested with 3 mg under high purity nitrogen atmosphere.

Nonisothermal Crystallization. The nonisothermal DSC scans were used to determine the peak crystallization temperature and the peak melt temperature of PA1012 with different MFIs. The procedure can be described as follows. The samples were firstly melted for 3 min at 230 ºC to erase thermal history and crystalline memory, then cooled down to 30 ºC at 10 ºC/min and held at 30 ºC for 3 min. Finally, the samples were heated at 10 ºC/min up to 230 ºC.

Thermal Fractionation by SSA[29-31]. SSA should be designed by employing the ideal self-nucleation (SN) temperature[30] ($T_{s,ideal}$) as the first $T_{s,1}$. Before the SSA procedure, SN[32-33] was performed to find $T_{s,ideal}$, which was described in Figures S1-S3. When comparing a series of PA1012 samples with different MFIs, the highest $T_{s,ideal}$ for the different samples can be used as a constant $T_{s,1}$ for all the samples. According to the results, the $T_{s,ideal}$ of the largest MFI was 192 °C and of which the smallest MFI was 191 °C. These results were reasonable because normally the sample with the highest $T_{s,ideal}$ corresponded to the sample with the highest T_m. We applied the same $T_{s,ideal}$ to all samples, i.e., 192 °C. The SSA procedure is described in Figure 1a[19]:

(a) The sample was melted for 3 min at 220 °C to erase the thermal history and

crystalline memory.

(b) Then, it was cooled at 20 °C/min down to 100 °C to create a standard semi-crystalline state, and it was held for 3 min at 100 ºC for thermal equilibration.

(c) The sample was heated from 100 ºC at 20 °C/min up to a chosen T_s and held there for 5 min. Therefore, 5 min was the selected fractionation time.

(d) Then, it was again cooled at 20 °C/min down to 100 °C so that the fraction of the sample that was melted at T_s crystallized during cooling.

(e) Steps (c) and (d) were repeated at progressively lower T_s values. The interval between T_s temperatures, or the fractionation window, was set as 5 °C. The total number of T_s temperatures (including $T_{s,1} = T_{s,ideal}$) applied to each sample was 5.

(f) Finally, the sample was heated at 20 °C/min up to 220 °C to obtain the thermally fractionated sample DSC heating scan.

The final heating DSC scan revealed the SSA fractionation profile of the sample. Since no annealing occurred at $T_{s,ideal}$, the number of produced fractions was equal to four.

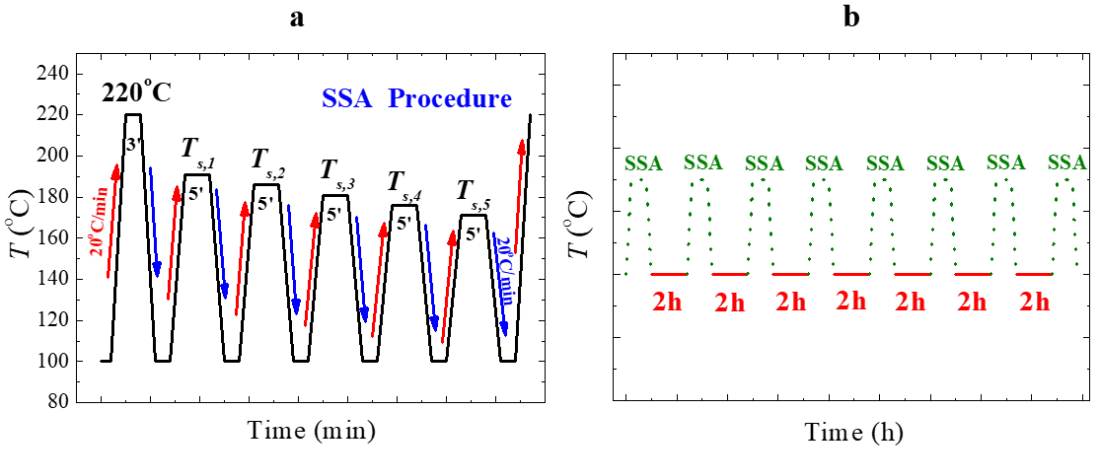

Figure 1. Experimental diagram: (a) Schematic representation of the SSA thermal protocol. (b) Combination of the SSA procedure and isothermal heat treatment for studying the lamellar thickness evolution and kinetics of PA1012. The procedures were the same as that employed in reference[20].

Kinetic Studies of PA1012 chains structural evolution by SSA. The combination of the SSA procedure and isothermal treatment at high temperatures for studying the lamellar thickness evolution (through the changes in the thermal fractionation profile) and kinetics for PA1012 was carried out in the DSC instrument. The N_2 atmosphere in DSC provided inert protection and removal of small molecular condensates. The procedure is described in Figure 1b. In the schematic diagram, the green line represents a complete SSA process, and the red line represents 2 h of isothermal treatment at a specific temperature. Each SSA revealed the fractionation of the sample after the cumulative isothermal treatment time at high temperatures. The total time of isothermal heat treatment was 14 h. The isothermal temperatures were set as 170 and 250 °C

separately. We studied *in situ* the changes in the lamellar thickness and its distribution evolution (through the evolution of the thermal fractionation profile) of the series of PA1012s.

Rheological Measurements

Oscillatory shear experiments were performed with a Discovery Hybrid Rheometer (TA DHR-II) using parallel plates with diameters of 25 mm. Oscillation time sweep experiments were performed at 210 °C with a frequency of 0.09 rad/s (Figure S4) and an amplitude of 10 % (Figure S5) in the linear viscoelastic regime with a continuous purge of nitrogen gas.

RESULTS AND DISCUSSION

Evolution of Lamellar Thickness and Its Distribution at Different Treating Temperatures for PA1012 Samples with Different MFIs

The longer the polymerization time, the lower the MFI value of the obtained sample. To clearly understand the relationship between MFI and molecular weight of PA 1012 samples, the relationship between number average molecular weight and MFI value is plotted in Figure 2. As expected, the number average molecular weight was negatively correlated with the MFI values, i.e., the higher the MFI value, the lower the molecular weight.

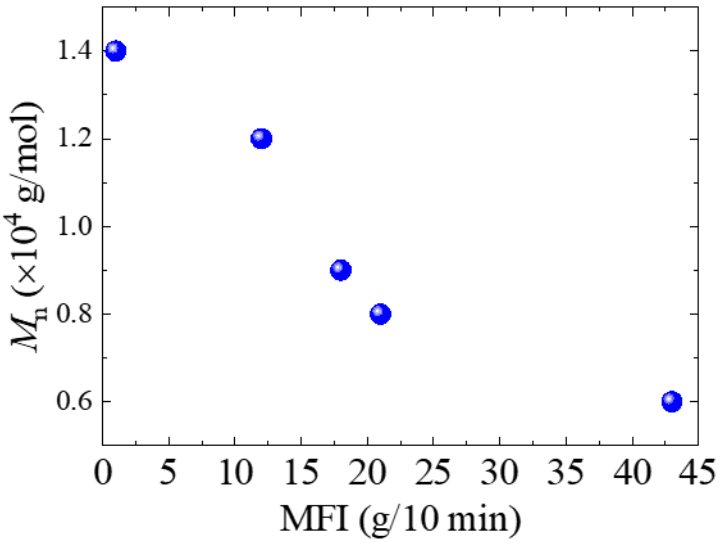

Figure 2. Number average molecular weight as a function of MFI value for PA1012.

We studied *in situ* the changes in the melting point distribution or SSA fractionation profile variations for the PA1012 samples with different MFIs when they were subjected to thermal conditioning at 170 °C and 250 °C. Figures 3 and 4 separately show the final DSC heating scans determined after the indicated cumulative isothermal treatment times at 170 and 250 °C. The melting enthalpy of the first ($\Delta H_{m1}/\Delta H_m$) or the last three ($\Delta H_{m2+\ m3+\ m4}/\Delta H_m$) thermal fractions normalized by dividing by the total melting enthalpy is plotted as a function of isothermal treatment time in Figure 5.

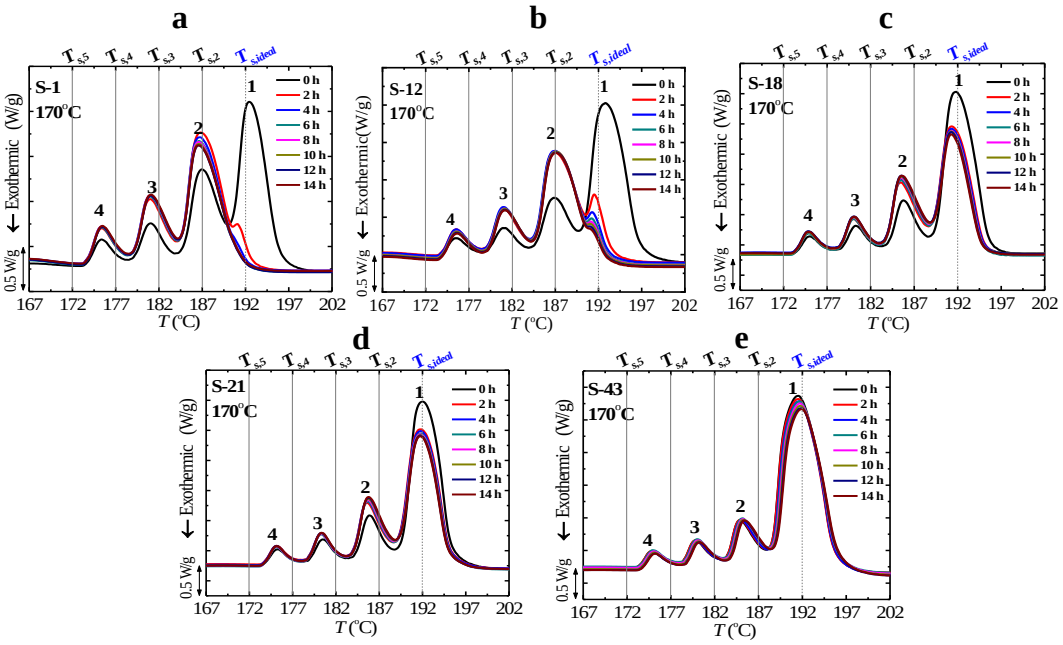

Figure 3. Final DSC heating scans (performed after SSA) after the indicated cumulative isothermal heat treatment times at 170 °C for the (a) S-1, (b) S-12, (c) S-18, (d) S-21, and (e) S-43 samples. The thermal fractions are numbered from 1 to 4 on top of each melting peak.

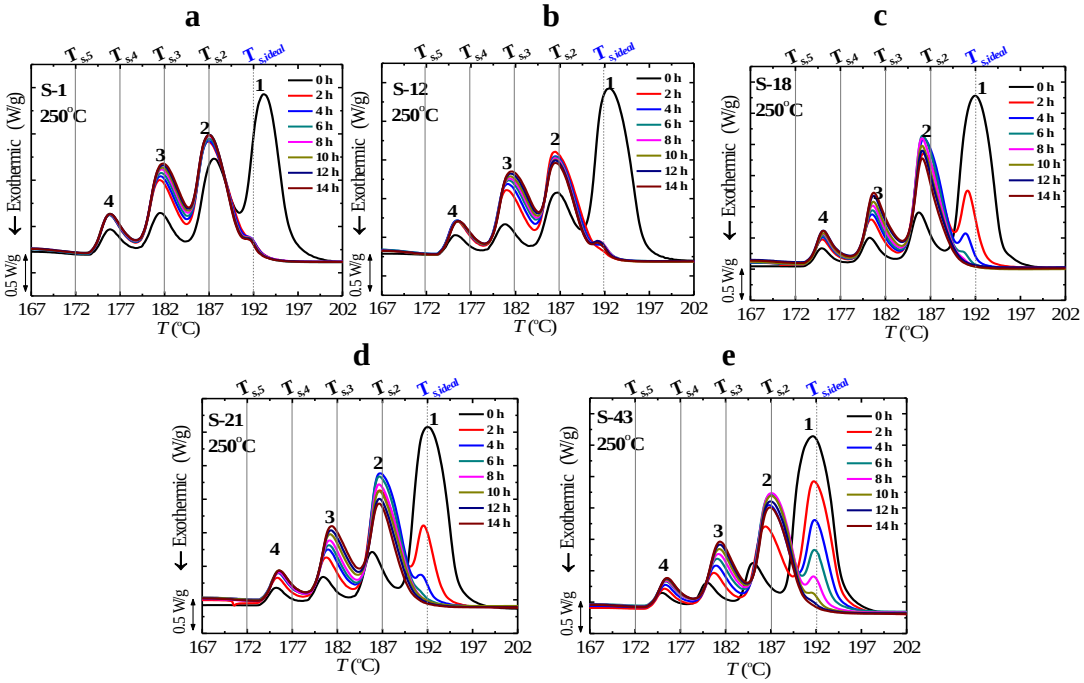

Figure 4. Final DSC heating scans (performed after SSA) after the indicated cumulative isothermal heat treatment times at 250 °C for the (a) S-1, (b) S-12, (c) S-18, (d) S-21, and (e) S-43 samples. The thermal fractions are numbered from 1 to 4 on top of each melting peak.

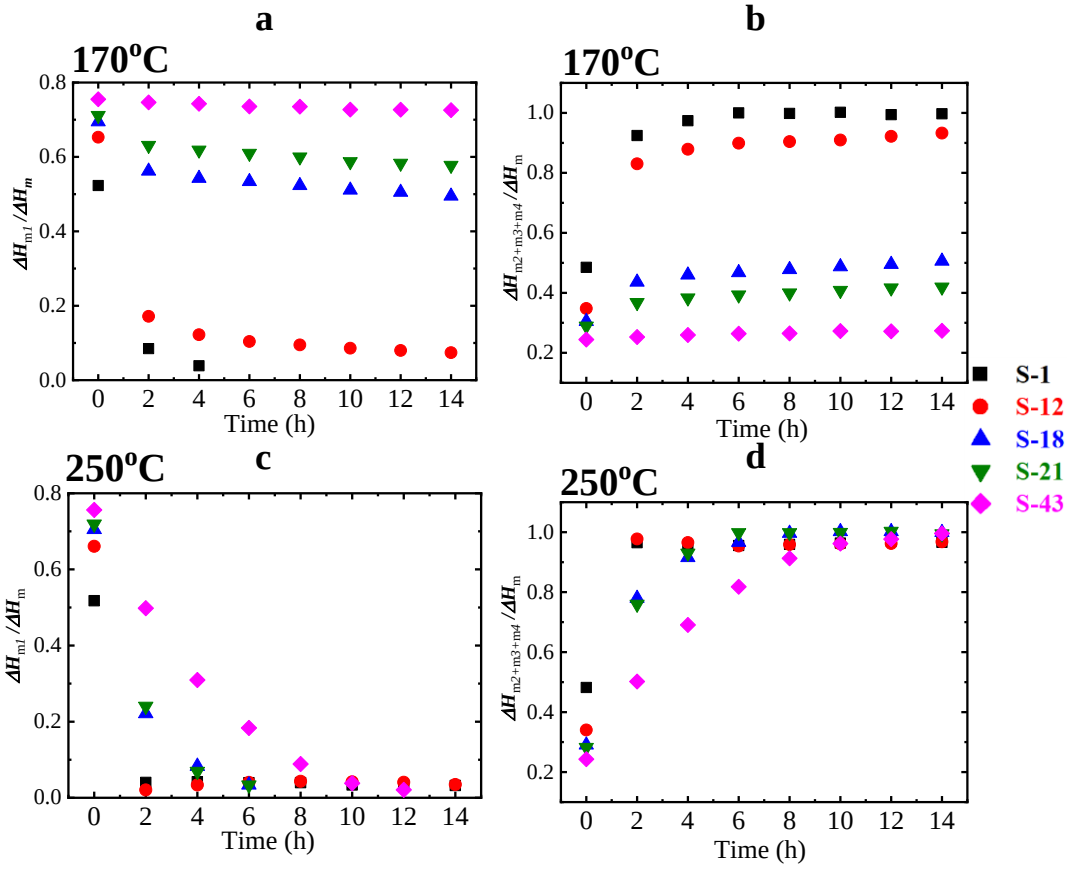

Figure 5. Melting enthalpy of the (a) (c) first ($\Delta H_{m1}/\Delta H_m$) or the (b) (d) last three ($\Delta H_{m2+\,m3+\,m4}/\Delta H_m$) thermal fractions divided by the total melting enthalpy as a function of isothermal time at 170 and 250 °C for the samples. The numbers are corresponding to the order of the thermal fractions in Figure 3 and 4.

The MFI is a numerical value indicating the flow capacity of plastic materials. The increase of MFI value is directly related to a decrease in melt viscosity (and a decrease in M_n, as indicated in Figure 2). The higher the chain diffusion or mobility in the melt, the higher the MFI value is. As molecular weight increases, entanglement density and melt viscosity increase. Even after polyamides finish their primary polymerization process, some reactive groups remain in the system, such as end-amino groups, end-

carboxylic groups, and potential cross-linking sites (secondary amines). Potential crosslinking sites could easily react with end groups to generate chemical crosslinking. Carboxylic end groups could react with amine end groups resulting in linear chain growth. After SSA, we define the highest melt temperature peak as the first thermal fraction and the lowest temperature peak as the fourth fraction (see the numbers in Figures 3 and 4). Here we set five T_s values to obtain four fractions, which was with high efficiency and reduced the influence of SSA in heat treatment to a larger extent. These four fractions had different average the melting points, and their four melting peaks can be considered to have four different average lamellar thicknesses, as proven earlier in different materials by small-angle X-ray scattering (SAXS)[25, 30] and we also used the Gibbs-Thomson equation to generate a distribution of lamellar thicknesses by employing the PA1012 DSC trace obtained after the SSA treatment[20].

As the initial molecular weight of PA1012 increased at lower thermal treatment temperature (i.e., 170 ºC, where the sample is in the semi-crystalline state), both the melting point and the melting enthalpy of the first fraction decreased fast, as shown in Figure 3 and Figure 5a. This was caused by the dominant chemical crosslinking reactions (see Scheme 1a below), which caused after SSA a decrease in the melting enthalpy of the first fraction without any subsequent increase during the cumulative thermal conditioning steps. The crosslinking reactions under these thermal protocol were proven in our previous work[20]. The work showed that chemical crosslinking was easily accomplished with end groups that rapidly reacted with active sites and the

crosslinking points occurred at the N atoms of PA1012, which was confirmed by the CPMAS ^{15}N NMR spectra and was similar to PA66[22]. Crosslinking interrupted the linear crystallizable sequences of PA1012, and hence fraction number 1, where the thickest lamellar crystals melt, tended to reduce its melting enthalpy and eventually almost disappeared for sample S-1 (Figure 3a). The shorter linear chains in between crosslinking points can only form thinner lamellae that do not melt in fraction number 1 but in lower melting point thermal fractions (i.e., 2, 3 or 4). Figures 5a and 5c represent trends that are mirror images of those in Figures 5b and 5d. The reason for this behavior is that the last three thermal fractions grow at the expense of the decrease in the first fraction.

At 170 °C (at $T<T_m$), the reaction rate increased as the initial molecular weight of the sample increased. The higher the initial molecular weight was (i.e., lower MFI), the lower the degree of crystallinity achieved, and the number of active end-groups, which were in the amorphous region and could move without the limit of the crystal lattice, was higher. A decrease in the crystallinity degree with a decrease in MFI can be observed in Figure 6. Figure 6 shows that the melting enthalpy increased as the initial molecular weight of the sample was lower (i.e., higher MFI). For PA1012 samples with higher MFI, because their low molecular weight chains are easier to enter the crystal lattice, many end-groups could be confined at the fold surface and reduce their activity (see Scheme 1a below).

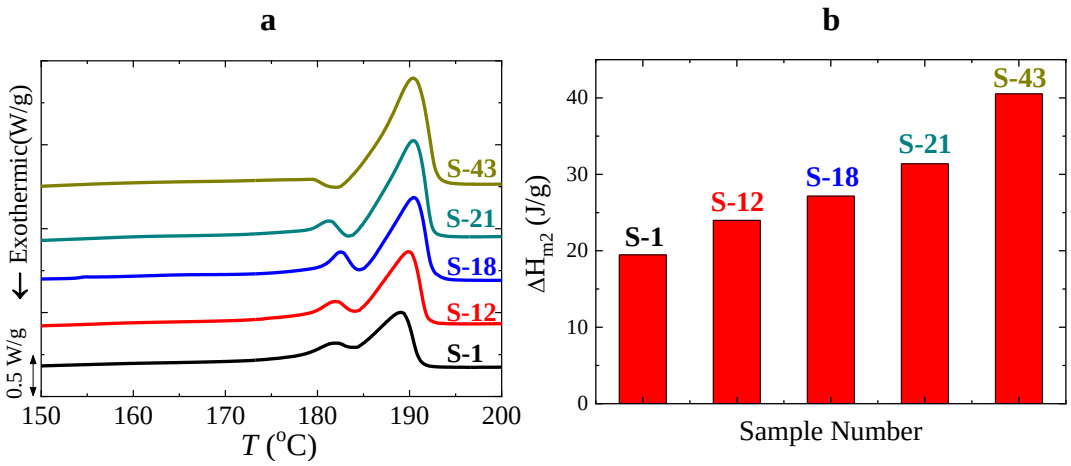

Figure 6. (a) DSC heating scans and (b) Melting enthalpy for PA1012 with different MFIs.

Using higher temperatures to thermally conditioning the samples, the changes were different. At 250 °C ($T>T_m$), the samples are in the melt, so the previous degree of crystallinity of the samples will not have any influence. The structural changes observed in the samples strongly depended on their initial melt viscosity and end group concentration. Figure 7 shows that the initial complex melt viscosity was lower as the molecular weight decreased (i.e., higher MFI values), as expected. In Figure S6, we could see that the end group concentration was positively correlated with the MFI values, i.e., the higher the MFI value, the higher the end group concentration.

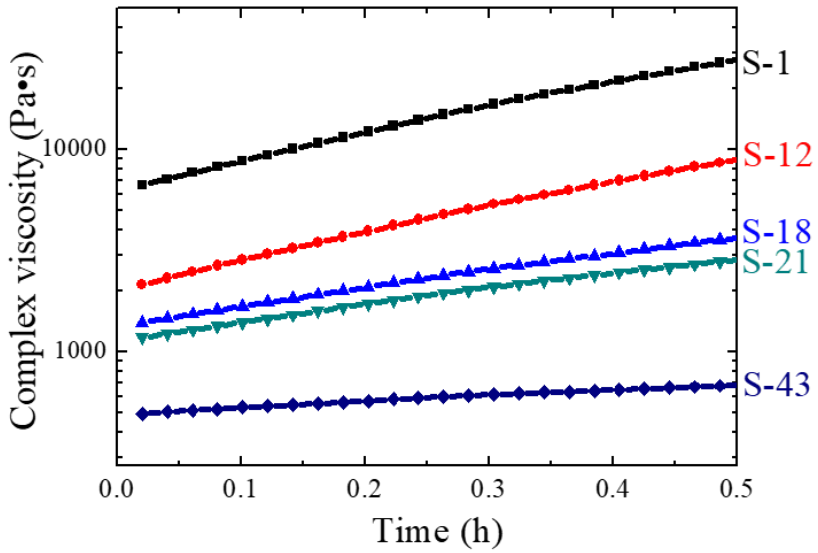

Figure 7. Oscillation time sweeps at 210 °C (>T_m) of PA1012 with different MFIs.

For lower MFIs samples (Figures 4a, b), the diffusion of end groups was slow due to the high melt viscosity and the end group concentration was small, which resulted in slow linear chain growth rate at shorter times. Therefore, chemical crosslinking predominated with fewer end groups that rapidly reacted with active sites at the beginning of the thermal treatment (Scheme 1b), which resulted in a decrease in the melting enthalpy of the first fraction (Figures 4a, b). With increasing time, the number of end groups rapidly increased and linear chain growth started to dominate via reactions of chain end groups (see Scheme 1b). Thus, the melting enthalpy of the first fraction slightly increased (Figure 5c). Although in Figure 4a, there seemed to be no increase in the melting enthalpy of the first fraction. To better show this small increased in the first fraction melting enthalpy, we included an additional isothermal treatment time of 0.5 h at 250 °C for sample S-1 (Figure 8). It was found that a slight minimum appeared in the plot of the melting enthalpy of the first thermal fraction versus time

(Figure 9). That meant that also for sample S-1, chemical crosslinking predominated initially and linear chain growth was dominant later, a behavior that was similar to that of sample S-12. The lower the MFI is, the earlier the time corresponding to the appearance of the minimum value.

For higher MFIs (Figure 4c-e), the diffusion of end groups was quick and the end group concentration was high, resulting in a quick linear chain growth rate. At shorter times, linear chain growth and crosslinking occurred in parallel (Scheme 1c). In terms of probability, end groups could react with potential crosslinking sites or other end groups. This was reflected in the decrease of the melting enthalpy of the first fraction (Figure 4 and 5c) and at the same time the increase in the melting points and melting enthalpies of the last three fractions. At longer times, crosslinking dominated again (Scheme 1c), making the melting enthalpy of the first fraction decrease and the last three fractions increase (Figures 5c and 5d).

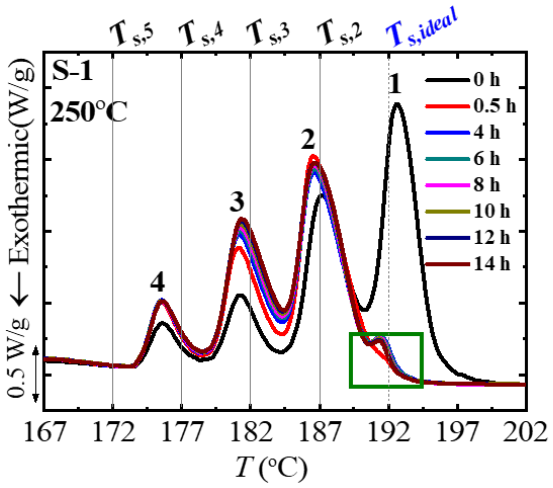

Figure 8. Final DSC heating scans (performed after SSA) after cumulative isothermal heat treatment time inserting 0.5 h between original 0 h and 4 h at 250 °C for sample S-1.

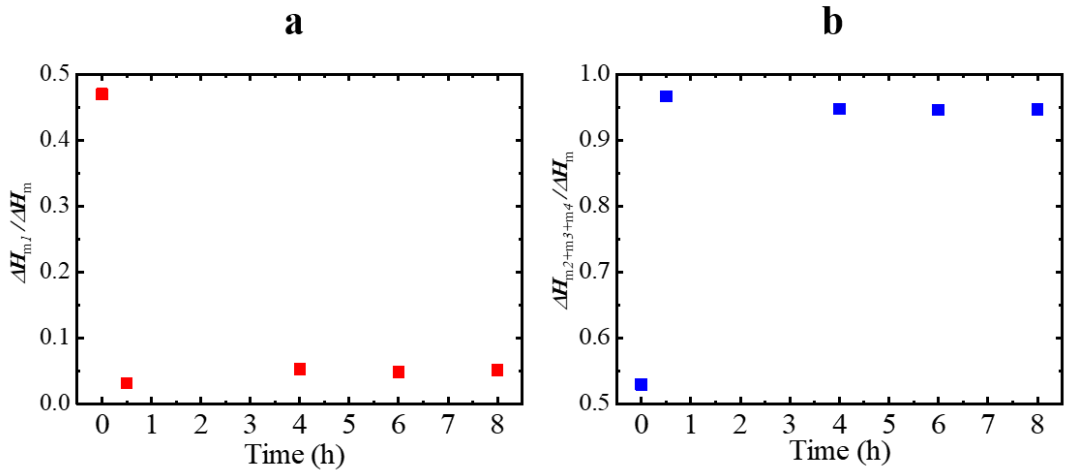

Figure 9. Melting enthalpy of the (a) first ($\Delta H_{m1}/\Delta H_m$) or the (b) last three ($\Delta H_{m2+m3+m4}/\Delta H_m$) thermal fractions against the total melting enthalpy as a function of isothermal time inserting 0.5 h between original 0 h and 4 h at 250 °C for sample S-1. The numbers are corresponding to the order of the thermal fractions in Figure 8.

Figure S6 shows that as the MFI value was higher, the end group concentration was higher. This also proves that by prolonging the polymerization time, the molecular weight and viscosity of the sample were increased by reducing the end group concentration in the reaction system. The reduction of the end group concentration caused slow amidation reaction between carboxylic end groups and amine end groups.

Mechanism for the Lamellar Thickness Evolution of PA1012 with Various Initial Molecular Weight at Different Thermal Treatment Temperature Ranges

Two structural changes, linear chain growth and chemical crosslinking, occurred during the isothermal treatments in the solid state and in the liquid state applied to PA1012 with different initial molecular weight. The influencing factor is different for PA1012 under different states as shown in Scheme 1.

When PA1012 samples were thermally treated at lower temperature (i.e., 170 ºC when the samples are in the semi-crytalline state), the structural evolution was limited by the previous crystalline structure. In this kind of situation (Scheme 1a), chemical crosslinking occurred primarily via reactions between potential crosslinking sites and end groups, which still remained in the system although the PA1012 samples had finished their primary polymerization process. As the initial molecular weight of PA1012 decreased (i.e., higher MFI), a higher degree of crystallinity limited the activity of end groups, which resulted in lower reaction rates.

When PA1012 samples were thermally treated at higher temperature (i.e., 250 ºC),

the structural evolution strongly depended on their initial melt viscosity and end group concentration and not on the previous degree of crystallinity, as the samples were melted at the treatment temperature. For higher initial melt viscosity and lower end group concentration of PA1012 (Scheme 1b, lower MFI), at the beginning of the thermal treatment, chemical crosslinking predominated with fewer end groups that rapidly reacted with active sites, because of slower end-group diffusion and lower end-group concentration. During the later stages (longer treatment times), the number of end groups rapidly increased, induced by chain scission under high temperature for long times, and linear chain growth started to dominate via reactions between chain end groups.

For lower initial melt viscosity and higher end group concentration of PA1012 (Scheme 1c, higher MFI), at shorter times, linear chain growth and crosslinking occurred in parallel; at longer times, crosslinking dominated again.

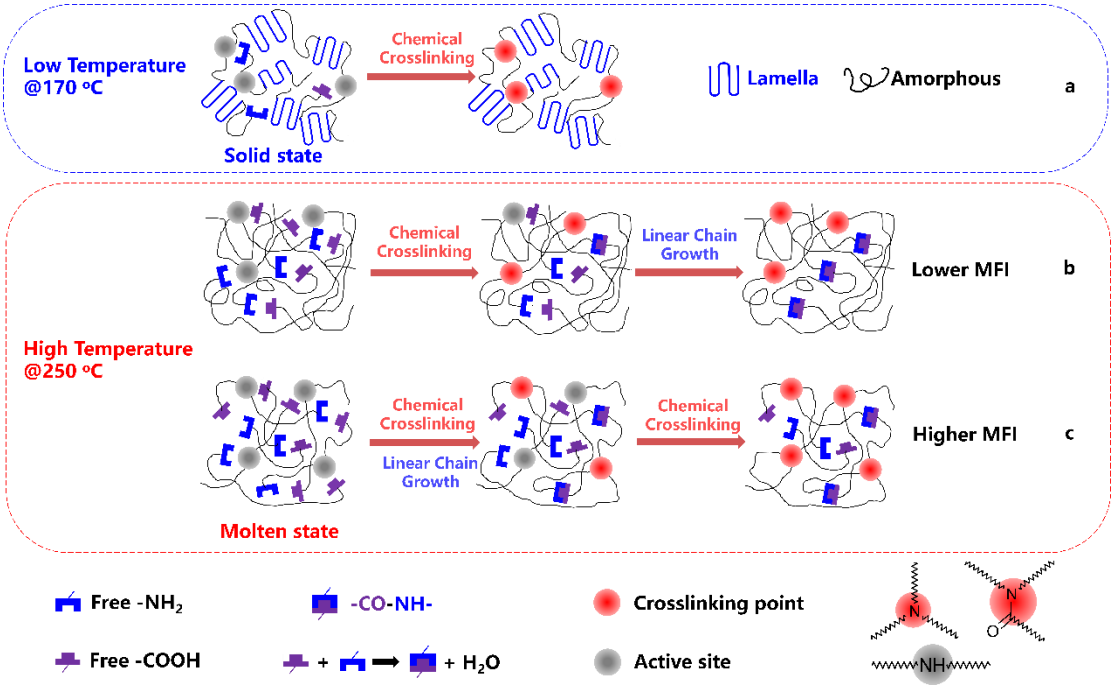

Scheme 1. Schematic of the Mechanism Competing by Linear Chain Growth and Chemical Crosslinking in PA1012 with different MFIs at 170 and 250 °C. At low temperature, chemical crosslinking occurs primarily for all PA1012 samples. But at high temperature, the mechanism varies from PA1012 with different MFIs, with chemical crosslinking or linear chain growth or both occurring in parallel.

CONCLUSIONS

In this study, the evolution of the melting points and its distribution of different PA1012s with different polymerization times was investigated by SSA. The results depended on the thermal treatment temperatures and on MFI values (i.e., molecular weight).

Thermally treating the samples below T_m, chemical crosslinking reactions

dominated, causing a decrease in the melting enthalpy of the first SSA thermal fraction. In the solid state, the structural evolution was mainly limited by crystallization. The high crystallinity achieved by the low molecular weight of PA1012 led to low crosslinking rates. Therefore, the lower the molecular weight of the PA1012 samples, the lower the crosslinking reaction rates.

Above T_m, the samples are in the melt, therefore the structural changes strongly depended on their melt viscosity and end group concentration. For lower MFIs, due to the high melt viscosity and low end group concentration, chemical crosslinking predominated with active sites that reacted with end groups at the beginning of the thermal treatment; with increasing time, linear chain growth occurred primarily via reactions of chain end groups. For higher MFIs, due to the low viscosity and high end group concentration, at shorter times, linear chain growth and crosslinking occurred in parallel; at longer times, crosslinking dominated again.

Based on the results obtained in the present work[20], we have further completed the investigation on how structural evolution of PA1012 by post-polymerization reactions triggered by thermal treatments occurs, as determined by different initial states. In our previous work[20], we have found that the structural changes occurring during thermal treatments enhanced toughness, strength, and heat resistance properties of PA1012. Therefore, this research could provide guidance for studies of thermal structural evolution of all AABB-type PAs and subsequent design of high-performance materials with different structures according to different application requirements. We could

obtain samples with very different structures according to selecting initial molecular weight, thermal treating temperatures and times.

ASSOCIATED CONTENT

Supporting Information

Protocols and plots of SN, oscillation amplitude sweep results, oscillation frequency sweep results, end group concentration results.

AUTHOR INFORMATION

Corresponding Author

*E-mail: alejandrojesus.muller@ehu.es and xiadong@iccas.ac.cn

ORCID

Xia Dong: 0000-0002-6409-7011

Alejandro J. Müller: 0000-0001-7009-7715

Dujin Wang: 0000-0002-2063-0873

Notes

The authors declare no competing financial interest.

ACKNOWLEDEMENTS

We acknowledge generous financial support from the following grants: National

Key R&D Program of China (2017YFB0307600) and the National Natural Sciences Foundation of China (21574140). A.J.M. acknowledges funding from the Basque Government through grant IT1309-19. We would like to thank the financial support provided by the BIODEST project, this project has received funding from the European Union's Horizon 2020 research and innovation programme under the Marie Sklodowska-Curie grant agreement No. 778092.

REFERENCES

1. Jones, N. A.; Atkins, E.; Hill, M. J.; Cooper, S. J.; Franco, L. Polyamides with a Choice of Structure and Crystal Surface Chemistry. Studies of Chain-Folded Lamellae of Nylons 8 10 and 10 12 and Comparison with the Other 2N 2(N + 1) Nylons 4 6 and 6 8. *Macromolecules.* **1997**, *30,* 3569–3578.

2. Li, Y.; Yan, D.; Zhu, X. Crystal forms of nylon 1012 crystallized from melt and after solution casting. *European Polymer Journal.* **2001**, *37,* 1849-1853.

3. Li, Y.; Zhu, X.; Tian, G.; Yan, D.; Zhou, E. Multiple melting endotherms in melt-crystallized nylon 10,12. *Polymer International.* **2001**, *50,* 677-682.

4. Li, Y.; Zhu, X.; Yan, D. Isothermal and nonisothermal crystallization kinetics of nylon 10 12. *Polymer Engineering & Science.* **2000**, *40,* 1989-1995.

5. Li, Y.; Zhang, G.; Zhu, X.; Yan, D. Isothermal and nonisothermal crystallization kinetics of partially melting nylon 10 12. *Journal of Applied Polymer Science.* **2003**, *88,* 1311-1319.

6. Li, X.; He, Y.; Dong, X.; Ren, X.; Gao, H.; Hu, W. Effects of hydrogen-bonding density on polyamide crystallization kinetics. *Polymer.* **2020**, *189,* 122165.

7. Zhou, C.; Qi, S.; Zhu, P.; Zhao, Y.; Xu, Y.; Dong, X.; Wang, D. The methylene infrared vibration and dielectric behavior monitored by amide group arrangement for long chain polyamides. *Polymer.* **2020**, *190,* 122231.

8. Telen, L.; Van, P., P.; Goderis, B. Random Copolymers from Polyamide 11 and Polyamide 12 by Reactive Extrusion: Synthesis, Eutectic Phase Behavior, and Polymorphism. *Macromolecules.* **2016**, *49,* 876-890.

9. Liu, S.; Yu, Y.; Cui, Y.; And, H. Z.; Mo, Z. Isothermal and nonisothermal crystallization kinetics of nylon-11. *Journal of Applied Polymer Science.* **1998**, *70,* 2371-2380.

10. Zhang, Q.; Mo, Z.; Liu, S.; Zhang, H. Influence of annealing on structure of Nylon 11. *Macromolecules.* **2000**, *33,* 5999-6005.

11. Gogolewski, S.; Czerntawska, K.; Gastorek, M. Effect of annealing on thermal properties and crystalline structure of polyamides. Nylon 12 (polylaurolactam). *Colloid and Polymer Science.* **1980**, *258,* 1130-1136.

12. Dencheva, N.; Nunes, T. G.; Oliveira, M. J.; Denchev, Z. Crystalline structure of polyamide 12 as revealed by solid-state13C NMR and synchrotron WAXS and SAXS. *Journal of Polymer Science Part B: Polymer Physics.* **2005**, *43,* 3720-3733.

13. Ma, N.; Liu, W.; Ma, L.; He, S.; Liu, H.; Zhang, Z.; Sun, A.; Huang, M.; Zhu, C. Crystal transition and thermal behavior of Nylon 12. *e-Polymers.* **2020**, *20,* 346-352.

14. Wang, D.; Shao, C.; Zhao, B.; Bai, L.; Wang, X.; Yan, T.; Li, J.; Pan, G.; Li, L. Deformation-Induced Phase Transitions of Polyamide 12 at Different Temperatures: An in Situ Wide-Angle X-ray Scattering Study. *Macromolecules.* **2010**, *43,* 2406-2412.

15. McFerran, N. L. A.; Armstrong, C. G.; McNally, T. Nonisothermal and isothermal crystallization kinetics of nylon-12. *Journal of Applied Polymer Science.* **2008**, *110,* 1043-1058.

16. Wang, L.; Dong, X.; Wang, X.; Zhu, G.; Li, H.; Wang, D. High performance long chain polyamide/calcium silicate whisker nanocomposites and the effective reinforcement mechanism. *Chinese Journal of Polymer Science.* **2016**, *34,* 991-1000.

17. Gao, Y.; Dong, X.; Wang, L.; Liu, G.; Liu, X.; Tuinea-Bobe, C.; Whiteside, B.; Coates, P.; Wang, D.; Han, C. C. Flow-induced crystallization of long chain aliphatic polyamides under a complex flow field: Inverted anisotropic structure and formation mechanism. *Polymer.* **2015**, *73,* 91-101.

18. Wang, Y.; Zhu, P.; Qian, C.; Zhao, Y.; Wang, L.; Wang, D.; Dong, X. The Brill Transition in Long-Chain Aliphatic Polyamide 1012: The Role of Hydrogen-Bonding Organization. *Macromolecules.* **2021**, *54,* 6835-6844.

19. Liu, X.; Wang, Y.; Liu, L.; Dong, X.; Wang, D. Time and Temperature Dependence of the Structural Evolution for Polyamide 1012. *Chinese Journal of Polymer Science.* **2020**, *38,* 993-998.

20. Zhou, C.; Dong, S.; Zhu, P.; Liu, J.; Dong, X.; Wang, D. Effects of Linear Alicyclic Polyamide Chemical Structure on the Mechanical and Optical Properties. *Acta Polymerica Sinica.* **2021**, *52,* 297-303.

21. Lai, Y.; Wang, Y.; Wang, L.; Li, X.; Zhao, J.; Dong, X.; Wang, D. Optical Inversion Characteristics of PA56 Spherulites. *Acta Polymerica Sinica.* **2020**, *51,* 1267-1274.

22. Schaffer, M.; Marchildon, E. K.; Mcauley, K. B.; Cunningham, M. F. Thermal Nonoxidative Degradation of Nylon 6,6. *Journal of Macromolecular Science: Reviews in Macromolecular Chemistry & Physics.* **2000**, *40,* 233-233.

23. Vouyiouka, S. N.; Karakatsani, E. K.; Papaspyrides, C. D. Solid state polymerization. *Prog. Polym. Sci.* **2005**, *30,* 10-37.

24. Li, X.; Wang, L.; Wang, D.; Müller, A. J.; Dong, X. Competition between Chain Extension and Crosslinking in Polyamide 1012 during High-Temperature Thermal Treatments as Revealed by Successive Self-Nucleation and Annealing Fractionation. *Macromolecules.* **2021**, *54,* 7552-7563.

25. Lorenzo, A. T.; Arnal, M. L.; Müller, A. J.; Boschetti de Fierro, A.; Abetz, V. High Speed SSA Thermal Fractionation and Limitations to the Determination of Lamellar Sizes and Their Distributions. *Macromolecular Chemistry and Physics.* **2006**, *207,* 39-49.

26. Lu, L.; Alamo, R. G.; Mandelkern, L. Lamellar Thickness Distribution in Linear Polyethylene and Ethylene Copolymers. *Macromolecules.* **1994**, *27,* 6571-6576.

27. Lorenzo, A. T.; Arnal, M. L.; Müller, A. J.; Lin, M.; Chen, H. SAXS/DSC Analysis of the Lamellar Thickness Distribution on a SSA Thermally Fractionated Model Polyethylene. *Macromolecular Chemistry and Physics.* **2011**, *212,* 2009-2016.

28. Safari, M.; Mugica, A.; Zubitur, M.; Martinez de Ilarduya, A.; Munoz-Guerra, S.; Müller, A. J. Controlling the Isothermal Crystallization of Isodimorphic PBS-ran-PCL Random Copolymers by Varying Composition and Supercooling. *Polymers (Basel).* **2019**, *12,* 17.

29. Müller, A. J.; Arnal, M. L. Thermal fractionation of polymers. *Progress in Polymer Science.* **2005**, *30,* 559-603.

30. Müller, A. J.; Michell, R. M.; Pérez, R. A.; Lorenzo, A. T. Successive Self-nucleation and Annealing (SSA): Correct design of thermal protocol and applications. *European Polymer Journal.* **2015**, *65,* 132-154.

31. Muller, A. J.; Hernandez, Z. H.; Arnal, M. L.; Sanchez, J. J. Successive self-nucleation/annealing (SSA): A novel technique to study molecular segregation during crystallization. *Polymer Bulletin.* **1997**, *39,* 465-472.

32. Michell, R. M.; Mugica, A.; Zubitur, M.; Müller, A. J., Self-Nucleation of Crystalline Phases Within Homopolymers, Polymer Blends, Copolymers, and Nanocomposites. In *Polymer Crystallization I: From Chain Microstructure to Processing*, Auriemma, F.; Alfonso, G. C.; de Rosa, C., Eds. Springer International Publishing: Cham, 2017; pp 215-256.

33. Sangroniz, L.; Cavallo, D.; Müller, A. Self-Nucleation Effects on Polymer Crystallization. *Macromolecules.* **2020**, *53,* 4581–4604.